JOM, Vol. 68, No. 12, 2016
DOI: 10.1007/s11837-016-1966-2

Acoustic Emission as a Tool for Exploring Deformation Mechanisms in Magnesium and Its Alloys In Situ

ALEXEI VINOGRADOV[1,2,4] and KRISTIAN MÁTHIS[3]

1.—Department of Engineering Design and Materials, Norwegian University of Science and Technology – NTNU, Richard Birkelandsvei 2B, 7491 Trondheim, Norway. 2.—Institute of Advanced Technologies, Togliatti State University, 445667 Togliatti, Russia. 3.—Department of Physics of Materials, Charles University, Ke Karlovu 5, 121 16 Prague, Czech Republic. 4.—e-mail: alexei.vinogradov@ntnu.no

Structural performance of magnesium alloys depends strongly on specific deformation mechanisms operating during mechanical loading. Therefore, in situ monitoring of the acting mechanisms is a key to performance tailoring. We review the capacity of the advanced acoustic emission (AE) technique to understand the interplay between two primary deformation mechanisms—dislocation slip and twinning—in real time scale. Details of relative contributions of dislocation slip and deformation twinning to the mechanical response of pure Mg and Mg-Al alloy are discussed in view of AE results obtained with the aid of recently proposed spectral and signal categorization algorithms in conjunction with with neutron diffraction data.

INTRODUCTION

Having a hexagonal closed packed (hcp) structure and ratio of the crystallographic axes c/a close to $\sqrt{8/3}$, the deformation behavior of magnesium alloys is rather different from other hcp metals. At room temperature, besides the most easily activated $(0001)\langle 11\bar{2}0\rangle$ basal slip the activation of first-order $\{10\bar{1}0\}\langle 11\bar{2}0\rangle$ prismatic and first-order pyramidal ($\{10\bar{1}1\}\langle 11\bar{2}0\rangle$) slip systems has been observed.[1] The second-order ($\{11\bar{2}2\}\langle \bar{1}\bar{1}23\rangle$) pyramidal slip system generally requires either higher applied stress and/or elevated temperatures to be activated.[1] Accommodating plastic strain in a polycrystalline specimen requires activation of at least five independent deformation modes. The combination of all systems having $\langle a\rangle$ (i.e. $\langle 11\bar{2}0\rangle$) direction provides at best four independent slip systems. Further, the $\langle c+a\rangle$-slip in the second-order pyramidal system has a high critical resolved shear stress (CRSS) at ambient temperatures.[2] Thus, deformation twinning is preferred mechanism that accommodates the deformation in line with the von Mises rule.

In magnesium, the most easily activated twinning modes are $\{10\bar{1}2\}$ extension and $\{10\bar{1}1\}$-type compression twinning.[3] The twinning on $\{10\bar{1}2\}$ plane is associated with extension along the c-axis and reorientation of the lattice by 86.3°. The $\{10\bar{1}1\}$ compression twinning results in contraction along the c-axis and tilting of the lattice by 56°. Formation of $\{10\bar{1}1\}$-$\{10\bar{1}2\}$-type double-twins have been also reported in the literature and identified as one of the mechanisms leading to failure.[4]

Experimental Methods for Investigation of Deformation Mechanisms in Magnesium Alloys

Various experimental techniques are used to investigate the twinning and dislocation slip in magnesium alloys. Optical and electron microscopy are among the most often used methods. The behavior of extension twins can be observed to some extent in optical microscope. The twinned area can be evaluated according to the ASTM E5620-2 standard. Much more details are provided by the electron backscatter diffraction (EBSD) technique disclosing, in particular, orientation relations between twins and parent grains. The advantage of EBSD over other methods of observation (e.g., optical or secondary electron image acquisition) is that the local crystalline microstructure can be characterized using orientation information with higher spatial resolution.[5] Moreover, the method

(Published online June 2, 2016)

gives access to the internal stress distribution at twin boundaries through the kernel misorientation maps.

The investigation of the dislocation structure is usually a more complex task, which is performed by transmission electron microscopy. However, the dislocations tend to form tangles, which complicates their proper identification. Particularly, getting information about $\langle c + a \rangle$-dislocations is difficult because of their low population and a tendency to decompose to $\langle a \rangle$ and $\langle c \rangle$ components. Therefore, pure $\langle c + a \rangle$-slip has been studied either in single crystals[6] or in textured materials, where compression along the crystallographic c-axis is the dominant deformation mode.[7] These tests require precise sample orientation, since even a small ($>5°$) deviation causes additional basal slip and twinning, which interferes the observation.[6]

Recently, the EBSD assisted slip trace analysis (STA) performed in a scanning electron microscope (SEM) is used to get a deeper insight into the activity of different slip systems.[8] In this method, first, orientations of the investigated grains are determined with the EBSD method. In the next step, the specimen is deformed up to a given level of strain, and the slip traces are observed by secondary electron imaging. Finally, post-mortem EBSD mapping is performed to determine the orientation development of those grains, in which slip traces were detected. Based on this information the traces are assigned to particular slip systems. This method works well for materials with grain sizes below 20 μm, where the slip lines are well defined and the number of examined grains is statistically representative. In the specimens with larger grains a more diffuse slip pattern develops complicating the analysis and leading to less conclusive results.[8]

From the statistical point of view, the diffraction line profile analysis (DLPA) gives the best results.[9] In this procedure, the influence of dislocations on the peak broadening is evaluated. Each diffraction pattern is fitted by the sum of a background spline and the convolution of the instrumental pattern and the theoretical line profiles related to crystallite size and dislocations. As a result of the fitting procedure, the dislocation density and the fractions of dislocations in the different slip system families can be determined in a large specimen volume.[10]

In the last decade the in situ testing had come to the forefront. Offering instantaneous information about the ongoing deformation mechanisms, the in situ techniques reduce the impact of relaxation effects such as detwinning. Digital image correlation (DIC) is the most common technique for investigation of strain field distribution during deformation. However, if more detailed information is required, both STA and DLPA can be used in situ. The in situ STA is usually provided using a miniaturized deformation rig, which can be mounted into the vacuum chamber of a SEM.[8] In the case of DLPA the diffraction profile is recorded using a hard x-ray or neutron beam.[11] The essential advantage of the synchrotron radiation is its brilliance which makes it possible to obtain a high quality diffraction pattern in seconds.[12] The neutron diffraction technique is used when a larger specimen volume has to be investigated, which is a key issue for coarse grain (>50 μm) materials. Besides the information about active slip systems, the twinned volume can be evaluated from diffraction data.[13]

Survey of Acoustic Emission Technique as a Means for Characterization of Deformation Behavior of Magnesium Alloys

Providing excellent spatial resolution, the above reviewed experimental methods can be combined with acoustic emission measurements (AE), which complementary offers superior temporal resolution. The AE technique detects transient elastic waves generated by rapid energy release from localized sources within the material it is particularly sensitive for twin nucleation and collective dislocation motion. The time resolution of AE (few microseconds) is among the highest among currently available in situ techniques. Due to this fact, the potential of AE measurements as a deformation characterisation tool enjoys growing recognition nowadays.[14–16] For example, Chmelik and co-authors[17–23] investigated the influence of various metallurgical factors (texture, grain size and solute content) on AE and underlying twinning and dislocation slip behaviour under different loading modes (tension or compression) for Mg alloys AZ31, AZ61 and AZ80. The highest AE level was observed in a material with the biggest grains, which was explained by the larger size of mechanical twins that emerged and propagated within the grains. Similar conclusions were drawn by Li and Enoki.[24] These results provide a convincing illustration of the capability of the AE technique to investigate deformation mechanisms in a real time scale. However, in these studies the distinction between the AE footprints of the dislocation slip and twinning was argued mostly qualitatively. The capacity of the AE technique can further be dramatically enhanced through new methods of advanced signal processing. For example, Lu et al.[25] investigated the mechanical behaviour of extruded magnesium alloy AZ31B under uniaxial tensile loading using AE and hierarchical clustering and Kohonen's self-organising neural network map to discriminate between different deformation processes. They reported that (a) the breakaway of dislocations from solute atoms can be ruled out as a potent AE source since pure Mg exhibits the same AE features as alloy AZ31 and (b) no stress/strain threshold for AE exists, i.e. AE commenced immediately after the beginning of loading. Pomponi and Vinogradov have recently proposed a new non-supervised approach to AE signal categorisation.[26] This method, termed as

adaptive sequential k-means (ASK) clustering, allows in situ real-time monitoring of operative deformation mechanisms and distinguishing between them during plastic deformation and fracture of materials. Therefore, it should allow eliminating possible artefacts from twinning/de-twinning that may arise after specimen unloading in conventional *post-mortem* metallographic analysis of the microstructure after interrupted tensile or compression tests. This method was successfully used to clarify the relative roles played by two primary deformation mechanisms—dislocation slip and twinning—even when they operate concurrently during tensile[27] or cyclic[28] plastic deformation of wrought Mg alloys. In particular, it has been established that both deformation modes operate throughout the entire process of tensile loading in a commercial Mg-Zn-Zr alloy ZK60. The presence of their activity has been found to be independent of the initial grain size and texture. However, the contributions of each mechanism to the released AE energy have been found to be grain size dependent: in fine-grained materials, plastic deformation is initially carried by dislocation slip, but deformation twinning takes over as the lead mechanism early on. In a coarse-grained counterpart of the material, this sequence is reversed. Twinning in Mg and its alloys has been studied extensively in association with specific deformation asymmetry.[16,19,28,29] All in all, the concurrent measurement of AE and diffraction methods has been found essential in elucidation of twinning mechanism in magnesium alloys.[11]

In the present paper, we endeavor to demonstrate the capability of the AE method for investigation of the plasticity in magnesium alloys. Several examples shown in the next sessions highlight the advantages of combination of AE with other experimental techniques in revealing fundamental deformation mechanisms in Mg.

EXPERIMENTAL

Pure Mg and binary Mg-9 wt.% Al (further referred as Mg9Al) were used for experiments. Since the grain size significantly influences the activity of deformation mechanisms, specimens with similar grain sizes of (100 ± 10) μm were prepared and investigated. The as-cast specimens were then solution heat treated for 24 h at 413°C and quenched into water. The diffraction studies of the initial states revealed completely random orientation distribution of crystallites in the microstructure.[30] The mechanical testing was carried out using cylindrical specimens with a diameter of 9 mm and gauge length of 20 mm. The in situ neutron diffraction (ND) measurements were carried out at the SMARTS engineering instrument in the Lujan Neutron Scattering Center.[31] The mutual orientation of the longitudinal axis of the sample and the incident beam was 45°. Two detector banks were positioned at ±90° to the incident beam in order to record diffraction patterns in both longitudinal and transverse directions with respect to the loading axis. Tensile tests were performed using a horizontal 250 kN capacity load frame in strain control mode with 1×10^{-3} s^{-1} strain rate. To collect ND data with good enough statistics, the tests were interrupted at predefined strain levels (0.1%, 0.5%, 1%, 2%, 3%, 4%, 5%, 6%) for approximately 70 min. The AE signal was acquired by a Physical Acoustics PCI-2 board. A broadband AE sensor from Dakel company was mounted apart from the gauge length using vacuum grease and an elastic band. The AE signal from the sensor was amplified by 60 dB in the frequency range 100–1200 kHz. The threshold level was set at 30 dB. The AE was recorded during uniaxial deformation under the same conditions as during in situ ND testing. To perform the AE signal categorization by the ASK algorithm, the continuously streamed data were sectioned into consecutive individual realizations and a Fourier power spectral density function was calculated for each realization using a Welch technique. These spectra were normilizaed to the total power per realization and then used as input information for ASK clustering which tried to join the signals with similar spectra into the compact groups and disjoin the signals having statistically different power spectral denstities.

RESULTS AND DISCUSSION

Acoustic Emission Testing

The stress–strain curves (Fig. 1) show that the Al content increases both the yield stress and ultimate tensile strength. The evolution of AE count rates (i.e. number of crossing of threshold level per second) with true strain and true stress is presented in Fig. 2a and b, respectively. The characteristic peaks in the vicinity of the yield point can be attributed to a synergic effect of twin nucleation and massive dislocation motion.[32] It is obvious that the peak is shifted towards higher stresses in the Mg9Al alloy. Above the yield point the count rate rapidly decreases, which is a consequence of the reduced mean free path for dislocation motion restricted by the increasing dislocation density and twin growth, which is not detectable by AE. Despite the almost same maximum value of count rate, the contribution of particular deformation mechanisms to this peak is different. The ASK analysis applied to the streaming data shows (Fig. 3) that in the pure Mg specimen the profuse twinning dominates in the AE time series. At variance with this observation, the non-basal slip prevails in the AE frequency spectra at lower strain in the Mg9Al specimen.

In summary, the mechanical tests and AE data indicate that the Al content enhances the non-basal slip and twinning seems to be hindered. In the next section these assumptions are verified using the neutron diffraction technique.

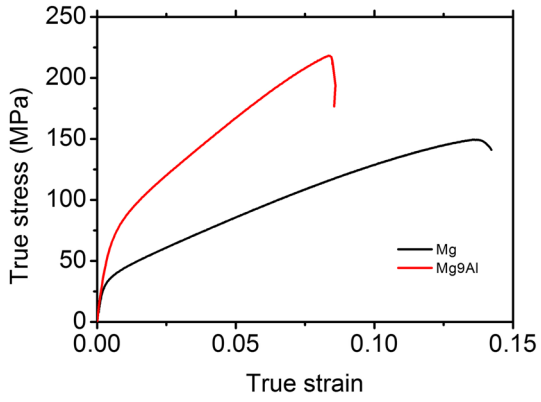

Fig. 1. The true stress–true strain curves as measured in tension for pure Mg and Mg + 9 wt.% Al specimens.

Solute Content Dependence of Twinned Volume

The evaluation of the twin volume fraction can be performed by a 2-bank Rietveld refinement assuming an axisymmetric texture. Since the initial texture is random and the uniaxial deformation is axisymmetric, the radial symmetry is warranted. The refinements were done using the SMARTS-ware[33] software packages developed at Los Alamos National Laboratory. Figure 4a indicates that the twin volume fraction is smaller for the Mg9Al alloy. Further, the growth of the twinned volume starts already at ~20 MPa in pure Mg, whereas it is noticeable only above 100 MPa in the Mg9Al alloy (Fig. 4b). The lower twin volume fraction in the Mg9Al alloy is caused by the solute—twin interaction. The solutes pin the twin dislocations thus impeding twin growth.[34] These results are in good agreement with AE findings showing that the share of twinning to plastic flow in the alloy is less significant than in pure Mg.

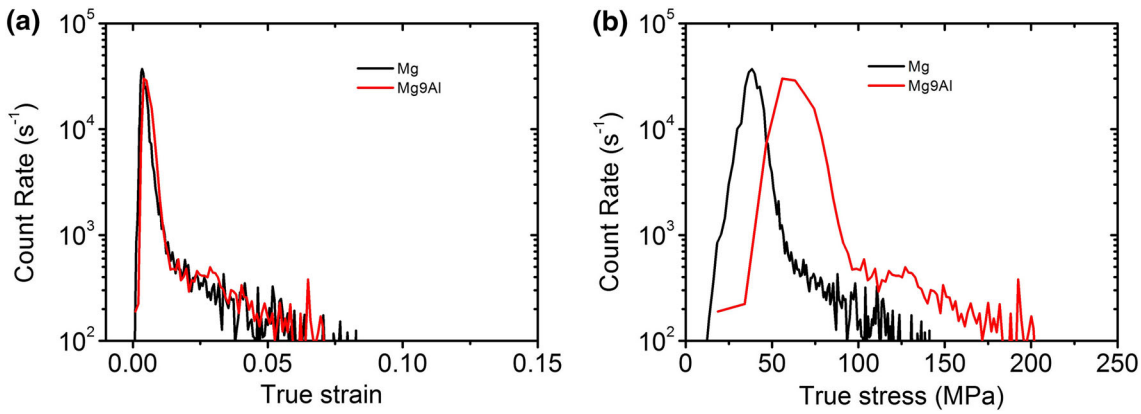

Fig. 2. The AE count rates measured during tension tests as a function of (a) strain; and (b) stress for pure Mg and Mg + 9 wt.% Al specimens.

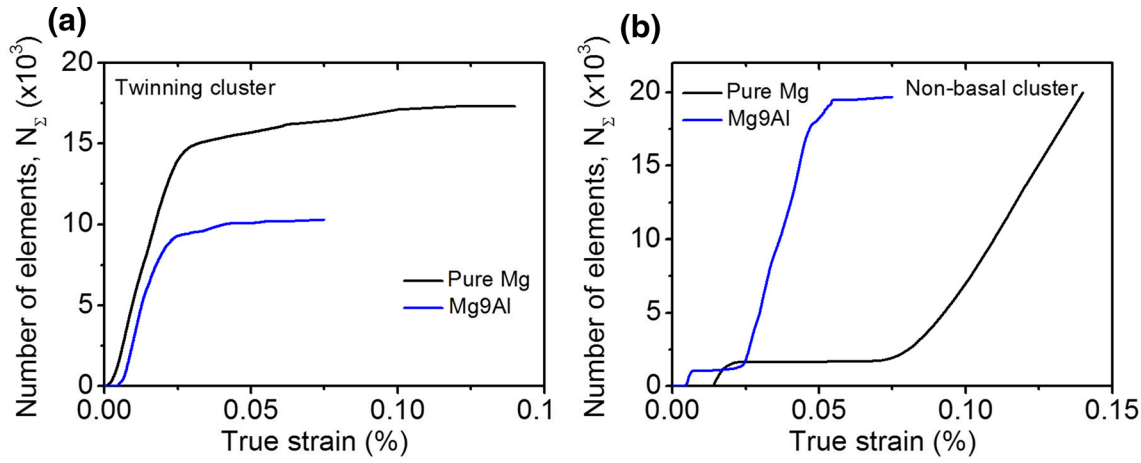

Fig. 3. Strain evolution of cumulative number of elements in the AE clusters assigned to (a) twinning; and (b) non-basal slip for pure Mg and Mg + 9 wt.% Al specimens.

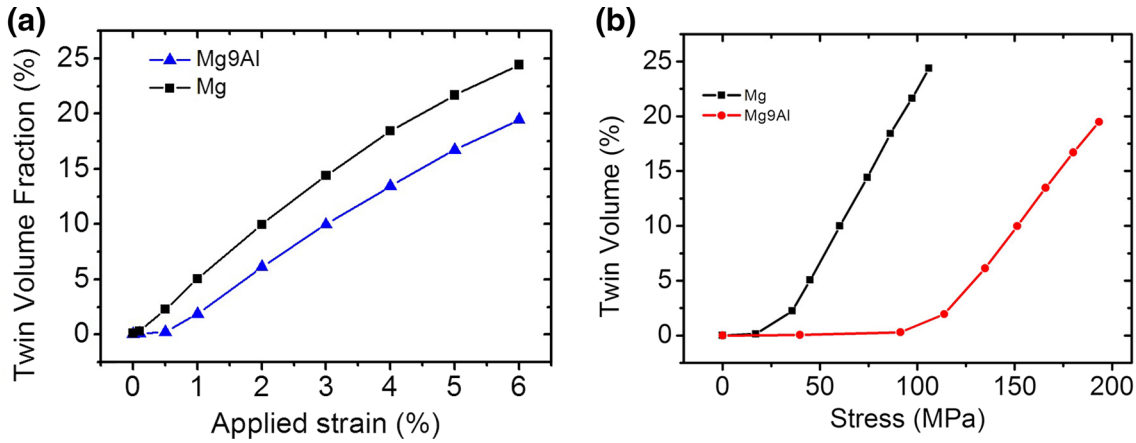

Fig. 4. Evolution of twin volume fraction as a function of (a) strain; and (b) stress.

Fraction of Dislocations in Particular Slip Systems

The neutron diffraction patterns obtained for the Mg samples deformed up to the strain of 6% were evaluated by the Convolutional Multiple Whole Profile (CMWP) fitting method.[35] Each diffraction pattern is fitted by the sum of a background spline, the convolution of the instrumental pattern and the theoretical line profiles related to crystallite size and dislocations. Finally, the dislocation density (ρ), and the parameters q_1^m and q_2^m are obtained. For magnesium, eleven families of slip systems on basal (4), prismatic (2) and pyramidal (5) planes with three different Burgers vectors are considered, which are divided into three groups based on their Burgers vectors: $b_1 = 1/3\langle\bar{2}110\rangle$ ($\langle a\rangle$ type), $b_2 = \langle 0001\rangle$ ($\langle c\rangle$ type) and $b_3 = 1/3\langle\bar{2}113\rangle$ ($\langle c + a\rangle$ type).

The *Hexburger* program was used for the fractions of dislocations in the different slip system families (f_a, f_c and f_{c+a}) from q_1^m and q_2^m.[10] It first selects some slip system families from $\langle a\rangle$ dislocation group and for these slip systems the weights are f_a. For other slip systems in this group the weights are zero. This procedure is also carried out for $\langle c\rangle$ and $\langle c + a\rangle$ Burgers vector groups where the non-zero weights are f_c and f_{c+a}, respectively. If these fractions have positive values the program stores them as one of the possible solutions. The number of the possible selections from the dislocation slip systems equals $(2^4 - 1)(2^2 - 1)(2^5 - 1) = 1395$. Finally, the positive solutions for the weights can be averaged for each slip system family, leading to the fractions of the eleven dislocation types. The fractions of the three Burgers vector groups, h_a, h_c and h_{c+a}, are obtained by the summation of the fractions of the related slip system families.

The strain dependence of the non-basal $\langle a\rangle$ versus basal $\langle a\rangle$-dislocations ratio is strongly influenced by solutes (Fig. 5). The fraction of non-basal $\langle a\rangle$ dislocations in the Mg9Al specimen increases at the expense of basal $\langle a\rangle$ dislocations more significantly than that in pure Mg. The role of prismatic $\langle a\rangle$ slip in macroscopic plasticity has been described in numerous theoretical and experimental works. Akhtar and Tegthsoonian showed that solute softening of prismatic slip system increases with increasing Al concentration in dilute Mg-Al single crystals.[36] Softening occurs through enhancing both the cross slip of dislocations and their ability to form jog-pairs.[37] The $\langle c + a\rangle$-slip is the only mechanism besides extension twinning, which provides elongation in c direction. However, its CRSS is significantly higher at room temperature in comparison with either basal or non-basal $\langle a\rangle$-slip.[2] The strain evolution of the ratio of $\langle a\rangle/\langle c + a\rangle$ dislocation is plotted in Fig. 6 (here, basal and non-basal $\langle a\rangle$-slip are considered together). For Mg9Al alloys at higher strain level the fraction of $\langle c + a\rangle$ dislocations significantly increases, whereas in pure Mg the significance of the 2nd order pyramidal slip is negligible. This difference can be substantiated by (i) softening of 2nd order pyramidal plane with

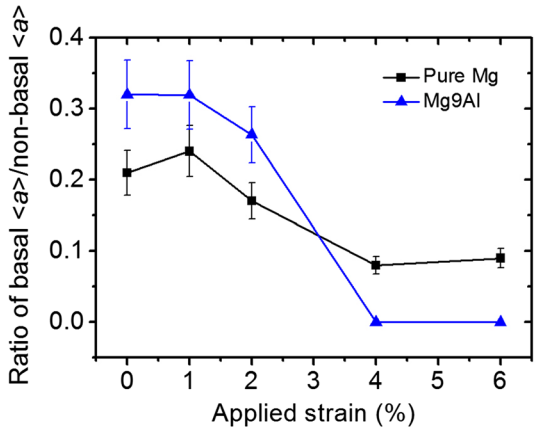

Fig. 5. Strain dependence of the basal $\langle a\rangle$—non-basal $\langle a\rangle$ dislocations ratio as a function of Al concentration.

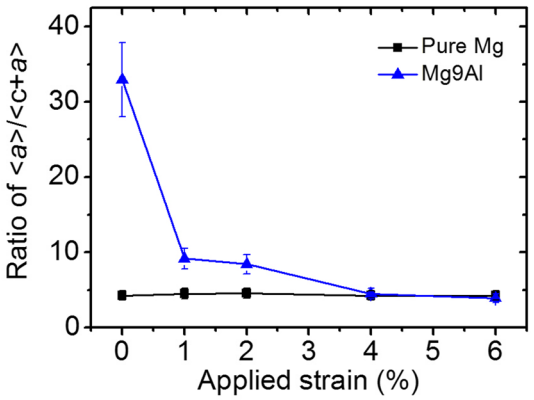

Fig. 6. Strain dependence of the $\langle a \rangle$-$\langle c + a \rangle$ dislocations ratio as a function of Al concentration.

solutes; (ii) restricted twin growth in Mg9Al. As a consequence, the local stress increases and an alternative mechanism in the form of $\langle c + a \rangle$-slip is activated in order to accommodate the strain.

CONCLUSION

In the foregoing sections, we presented a brief survey of acoustic emission (AE) technique as an in situ means of investigating deformation mechanisms in magnesium and its alloys. Although the original results were presented for pure Mg and Mg-9%Al alloy, the proposed methodology combining an advanced AE analysis and other in situ methods such as neutron diffraction can be applied to other materials without particular limitations if the kinetics of underlying deformation mechanisms is of concern.

Specifically, the influence of solute content on the deformation mechanisms was investigated in pure Mg and Mg-Al binary alloy and the following conclusion were drawn with an aid from AE measurements and neutron diffraction experiments:

- The solutes strongly affect the kinetics of twinning: the stress necessary for both twin nucleation and growth is higher if Al is present in magnesium specimens.
- The Al content leads to softening of both prismatic and pyramidal slip.
- As a consequence of constrained twin growth, the pyramidal $\langle c + a \rangle$ slip activates in Mg-9 wt.% Al alloy.

ACKNOWLEDGEMENTS

KM is grateful for the financial support of the Czech Science Foundation under the contract GB14-36566 and to Jan Čapek and Tomáš Krajňak for their kind help in data evaluation. AV appreciates the financial support from the Russian Ministry of Education and Science through the contract RFMEFI58615X0021.

REFERENCES

1. M.H. Yoo, *Metall. Trans. A* 12, 409 (1981).
2. A. Chapuis and J.H. Driver, *Acta Mater.* 59, 1986 (2011).
3. J.W. Christian and S. Mahajan, *Prog. Mater. Sci.* 39, 1 (1995).
4. M.R. Barnett, Z. Keshavarz, A.G. Beer, and X. Ma, *Acta Mater.* 56, 5 (2008).
5. A.J. Wilkinson and T.B. Britton, *Mater. Today* 15, 366 (2012).
6. T. Obara, H. Yoshinga, and S. Morozumi, *Acta Metall. Mater.* 21, 845 (1973).
7. S.R. Agnew, J.A. Horton, and M.H. Yoo, *Metall. Mater. Trans. A* 33, 851 (2002).
8. C.M. Cepeda-Jimenez, J.M. Molina-Aldareguia, and M.T. Perez-Prado, *Acta Mater.* 84, 443 (2015).
9. L.C. Dragomir, A. Borbély, and T. Ungár, *Eur. Powder Diffr.* 8, 95 (2004).
10. K. Máthis, K. Nyilas, A. Axt, I. Dragomir-Cernatescu, T. Ungár, and P. Lukáč, *Acta Mater.* 52, 2889 (2004).
11. K. Máthis, G. Csiszar, J. Čapek, J. Gubicza, B. Clausen, P. Lukáš, A. Vinogradov, and S.R. Agnew, *Int. J. Plasticity* 72, 127 (2015).
12. G. Garces, D.G. Morris, M.A. Munoz-Morris, P. Perez, D. Tolnai, C. Mendis, A. Stark, H.K. Lim, S. Kim, N. Shell, and P. Adeva, *Acta Mater.* 94, 78 (2015).
13. B. Clausen, C.N. Tome, D.W. Brown, and S.R. Agnew, *Acta Mater.* 56, 2456 (2008).
14. A. Vinogradov, I.S. Yasnikov, and Y. Estrin, *J. Appl. Phys.* 115, 233506 (2014).
15. A. Müller, C. Segel, M. Linderov, A. Vinogradov, A. Weidner, and H. Biermann, *Metall Mater. Trans. A* 1–16 (2015).
16. D. Drozdenko, J. Bohlen, S. Yi, P. Minárik, F. Chmelík, and P. Dobroň, *Acta Mater.* 110, 103 (2016).
17. T.T. Lamark, F. Chmelik, Y. Estrin, and P. Lukac, *J. Alloy. Compd.* 378, 202 (2004).
18. T.T. Lamark, F. Chmelik, Y. Estrin, and P. Lukac, *Kovove Mater.* 42, 293 (2004).
19. P. Dobron, F. Chmelik, J. Bohlen, K. Hantzsche, D. Letzig, and K.U. Kainer, *Int. J. Mater. Res.* 100, 888 (2009).
20. P. Dobron, F. Chmelik, J. Bohlen, D. Letzig, and K.U. Kainer, *Kovove Mater.* 43, 193 (2005).
21. J. Bohlen, F. Chmelik, P. Dobron, F. Kaiser, D. Letzig, P. Lukac, and K.U. Kainer, *J. Alloy. Compd.* 378, 207 (2004).
22. J. Bohlen, F. Chmelik, F. Kaiser, D. Letzig, P. Lukac, and K.U. Kainer, *Kovove Mater.* 40, 290 (2002).
23. J. Bohlen, P. Dobron, E.M. Garcia, F. Chmelik, P. Lukac, D. Letzig, and K.U. Kainer, *Adv. Eng. Mater.* 8, 422 (2006).
24. Y.P. Li and M. Enoki, *Mater. Trans.* 48, 1215 (2007).
25. Y. Lu, M. Gharghouri, and F. Taheri, *Nondestruct. Test Eval.* 23, 211 (2008).
26. E. Pomponi and A. Vinogradov, *Mech. Syst. Sig. Proc.* 40, 791 (2013).
27. A. Vinogradov, D. Orlov, A. Danyuk, and Y. Estrin, *Acta Mater.* 61, 2044 (2013).
28. A. Vinogradov, D. Orlov, A. Danyuk, and Y. Estrin, *Mater. Sci. Eng., A* 621, 243 (2015).
29. K. Máthis, J. Čapek, Z. Zdražilová, and Z. Trojanová, *Mater. Sci. Eng., A* 528, 5904 (2011).
30. K. Máthis, J. Čapek, B. Clausen, T. Krajňák, and D. Nagarajan, *J. Alloy. Compd.* 642, 185 (2015).
31. M.A.M. Bourke, D.C. Dunand, and E. Ustundag, *Appl. Phys. A* 74, S1707 (2002).
32. K. Máthis, J. Čapek, P. Harcuba, and V. Šíma, *Kovove Mater.* 51, 269 (2013).
33. B. Clausen, *SMARTSware Manual* (Los Alamos: The Regents of the University of California, 2003).
34. M. Ghazisaeidi, L.G. Hector, and W.A. Curtin, *Acta Mater.* 80, 278 (2014).
35. G. Ribárik, T. Ungár, and J. Gubicza, *Trans. Jpn. Inst. Met. Suppl.* 34, 669 (2001).
36. A. Akhtar and E. Teghtsoonian, *Trans. Jpn. Inst. Met. Suppl.* 9, 692 (1968).
37. C.H. Cáceres and D.M. Rovera, *J. Light Met.* 1, 151 (2001).